International Journal of Biological Macromolecules 135 (2019) 212–225

Contents lists available at ScienceDirect

International Journal of Biological Macromolecules

journal homepage: http://www.elsevier.com/locate/ijbiomac

A novel granulin homologue isolated from the jellyfish *Cyanea capillata* promotes proliferation and migration of human umbilical vein endothelial cells through the ERK1/2-signaling pathway

Chao Wang [a,1], Beilei Wang [a,1], Bo Wang [a,1], Qianqian Wang [a], Guoyan Liu [a], Chongxu Fan [b,*], Liming Zhang [a,*]

[a] Department of Marine Biotechnology, Faculty of Naval Medicine, Navy Medical University, Xiangyin Road No.800, Shanghai 200433, China
[b] Beijing Institute of Pharmaceutical Chemistry, Wennan Road No.59, Beijing 102205, China

ARTICLE INFO

Article history:
Received 19 March 2019
Received in revised form 15 May 2019
Accepted 16 May 2019
Available online 17 May 2019

Keywords:
Jellyfish
Granulin
Growth-promoting
Cell migration
Wound healing

ABSTRACT

Jellyfish grow rapidly and have a strong regenerative ability, indicating that they may express high levels of growth factors. Therefore, the aim of this research was to isolate the growth-promoting components from the jellyfish *Cyanea capillata* (*C. capillata*) and to further explore the underlying mechanisms. In this study, we first isolated and identified a novel polypeptide from *C. capillata* tentacles using size-exclusion chromatography followed by reverse-phase HPLC. This peptide, consisting of 58 amino acids (MW 5782.9 Da), belonged to the granulin (GRN) family of growth factors; thus, we named it *Cyanea capillata* granulin-1 (*Cc*GRN-1). Second, using CCK-8 assay and flow cytometry, we verified that *Cc*GRN-1 at the 0.5 μg/ml concentration could promote cell proliferation and increase the expression of cell-cycle proteins (CyclinB1 and CyclinD1). Third, signaling pathways studies showed that *Cc*GRN-1 could activate the PI3K/Akt- and ERK1/2 MAPK–signaling pathways but not the JNK MAPK- or NF-κB-signaling pathways. Subsequently, we further confirmed that the *Cc*GRN-1-induced cell proliferation and migration were associated only with the ERK1/2 MAPK–signaling pathway. Considering all of these factors, *Cc*GRN-1, as the first jellyfish-derived GRN homologue, possesses growth-promoting properties and may be a candidate for novel therapeutics to promote human wound healing in unfavorable conditions.

1. Introduction

Chronic wounds associated with diabetes, aging and cardiovascular diseases have become prevalent and are a costly healthcare problem globally [1]. These non-healing wounds can result in a high rate of disability and amputation because growth factors are deficient and wound surfaces have a high incidence of infection [2]. Moreover, chronic wounds can lead to long-term hospitalization which presents a huge financial burden for social community, family and the individual patients as well [3,4]. However, until now, few advanced therapeutics have been reported to effectively improve the healing outcomes. Therefore, safe, effective and affordable treatments must be developed for these chronic wounds.

Wound-healing is a complex process that depends on a multitude of growth factors and cytokines that regulate the signaling networks altering cell growth, differentiation, and metabolism [2,5]. Therefore, growth factor–based therapies have *expectedly* gained more attention, and some promising growth factors—such as the granulocyte-macrophage colony-stimulating factor (GM-CSF), vascular endothelial growth factor (VEGF), fibroblast growth factor (FGF), and platelet-derived growth factor (PDGF)—have been extensively studied and tested in wound repair [2,3,6]. However, topical delivery of growth factors must overcome some limitations such as short plasma half-life and susceptibility to degradation [2,7,8]. For example, epidermal growth factor (EGF), transforming growth factor beta (TGF-β) and PDGF are reported to be easily degraded by some proteases in the wounds [2]. To overcome these problems, some novel growth factor families should be explored. Fortunately, marine-derived bioactive peptides offer enormous potential as therapeutics because of their selectivity and high binding affinity with receptors to carry out signaling processes [9]. On the other hand, compared with terrestrial environments, marine ecosystems have some unique features—such as high salt, high pressure, low temperature and low-nutrient availability [10]—which may foster more structural novelty and biological diversities for developing promising drug candidates. As a representative of an abundant group of marine zooplankton, jellyfish (Scyphozoa) have received increasing attention for their complex life cycles and potential medicinal values in recent years. Generally, Scyphozoa have a special life cycle that typically incorporates both sexual and asexual proliferation, with sexual reproduction occurring at the medusa stage and asexual reproduction at the polyps phase [11]. Meanwhile, in unfavorable environmental conditions,

* Corresponding authors.
E-mail addresses: chongxu_fan@hotmail.com (C. Fan), lmzhang@smmu.edu.cn (L. Zhang).
[1] These authors contribute equally to this work.

https://doi.org/10.1016/j.ijbiomac.2019.05.101
0141-8130/

Scyphozoa also exhibit an unparalleled developmental plasticity that equips them to back-transform to immature from adult stages by body reorganization [12]. These flexible life cycles require a high rate of cell proliferation at different life stages and can be interpreted as an evolutionary outcome [13]. In addition, scientists have found that jellyfish grow rapidly and preserve a strong reproductive and regenerative capacity in response to the changing environment [11,12,14]. For example, after being attacked by predators or human beings, jellyfish undergo a rapid repair process and manifest a powerful regenerative ability. Their maximum growth rate reaches approximately 3 mm d^{-1} ($\pm$ 0.2 mm d^{-1}) [15], and their instantaneous growth rate exceeds 0.3 d^{-1} [16], which is possibly the highest rate ever recorded in epi-pelagic metazoans. Given these factors, we hypothesized that jellyfish expressed high levels of growth factors [13,17] and that further exploration of these active components would facilitate the development of novel drugs for wound healing. However, until now, isolation of the growth factors or their homologues from jellyfish has rarely been reported.

Cyanea capillata (*C. capillata*)—also called the "Sea Blubber", the "Hairy Stinger" or the "Snottie"—is a major jellyfish type found in southeast Chinese coastal waters [18]. In our previous study, we performed a *de novo* transcriptome sequencing of the tentacle tissue and obtained a well-categorized and annotated transcriptome of the jellyfish *C. capillata* [19]. Among these transcripts, four sequences were identified as being similar to VEGFs, which have been reported to stimulate angiogenesis and influence wound closure, epidermal repair, granulation tissue formation and repair quality [20,21]. On the other hand, in our preliminary experiments, we also provided evidence that tentacle extract (TE) from *C. capillata* could significantly promote the proliferation and migration of human umbilical vein endothelial cells (HUVECs), which may be mediated by ERK1/2 signal transduction [22]. Therefore, we have reasons to believe that some bioactive growth factors or their homologues are contained in TE. As a step forward, the present study aimed to isolate and purify these bioactive components from *C. capillata* tentacles, to investigate their possible biological functions through computational analysis, and finally to explore the corresponding mechanisms through biological assays.

2. Material and methods

2.1. Reagents

Human umbilical vein endothelial cells (HUVECs) were purchased from Zhongqiao Xinzhou Biotech (Shanghai, China). A Cell Counting Kit-8 (CCK-8) was purchased from Dojindo Molecular Technologies (Kumamoto, Japan). The antibodies Phospho-Akt (Ser473), Akt, Phospho-JNK (Thr183/Tyr185), JNK, Phospho-NF-κB (Ser536), NF-κB, Phospho-IκBα, CyclinB1 and CyclinD1 were purchased from Cell Signaling Technology (Beverly, MA, USA). Phospho-ERK1/2, ERK1/2, and GAPDH antibodies were purchased from Abcam (Cambridge, MA, USA). Beta-Tubulin, HRP-conjugated anti-rabbit IgG and anti-mouse IgG were purchased from Beyotime (Jiangsu, China). LY294002 (PI3K/Akt inhibitor), PD98059 (ERK1/2 inhibitor), SP600125 (JNK inhibitor) and Bay11–7082 (NF-κB inhibitor) were purchased from Selleck (Houston, TX, USA). FITC-conjugated goat anti-rabbit IgG and FITC-conjugated goat anti-mouse IgG were purchased from EarthOx Life Sciences (Millbrae, CA, USA). 4′, 6-diamidino-2-phenylindole (DAPI) was purchased from Beyotime (Jiangsu, China). Other chemical reagents were purchased from Sinopharm (Shanghai, China).

2.2. Cyanea capillata granulin-1 (CcGRN-1) isolation from the jellyfish C. capillata

2.2.1. Rapid preparative tentacle extract (rpTE) from the jellyfish C. capillata

C. capillata specimens were collected from the Sanmen Bay, East China Sea in June 2015 and identified by Professor Huixin Hong from the Fisheries College of Jimei University, Xiamen, China. The excised tentacles were preserved in a dry-ice chest and immediately shipped to Shanghai, where the samples were frozen at −70 °C until use. Thawed tentacles were mixed with ice-cold filtered seawater at a mass/volume ratio of 1:1 and stirred evenly. The mixture was centrifuged at 5000 ×*g* for 5 min, and the supernatant was decanted. The collected tentacles were washed again with seawater and immersed in phosphate-buffered saline (PBS, 0.01 M, pH 7.4) at a mass/volume ratio of 1:1. The mixture was vortex oscillated for 5 min and centrifuged at 5000 ×*g* for 5 min to remove the sediments. The supernatant was filtered through a dialysis bag (1000 Da, Spectrum, USA) against PBS for over 8 h. A subsequent centrifugation step at 4 °C and 10,000 × *g* for 10 min yielded the rapid preparative tentacle extract (rpTE). All procedures were performed at 4 °C, and rpTE was stored at −70 °C. Before use, rpTE was ultrafiltrated using an ultrafiltration tube (Millipore, USA) of a 30 kDa intercept molecular weight. The filtrate was dialyzed through a dialysis bag (1000 Da) against water for 24 h and then freeze-dried. The sample was finally dissolved in 50 mM acetic acid and filtered by a 0.45 μm filter membrane (Millipore, USA) for the next purification step.

2.2.2. Isolation and purification of CcGRN-1

The solution after pretreatment was first fractionated by a gel-filtration Superdex 30 (GE Healthcare, USA) column (800 × 16 mm), which was connected to an ÄKTA prime system (GE Healthcare, USA) and equilibrated with 50 mM acetic acid. The column was eluted with a flow rate of 1 ml/min, and eluates were collected in glass tubes at 5 ml per tube. The purified ingredients were further separated by high-performance liquid chromatography (HPLC) with an MZ-ANALYTICAL C8 (Mainz, German) column (250 × 4.6 mm). The latter was connected to an Agilent 1100 HPLC system (Agilent Technologies, USA) and eluted in a gradient of 0–40% (v/v) acetonitrile for 40 min in the presence of 0.1% (v/v) trifluoroacetic acid at a flow rate of 1 ml/min. Subsequently, the purified ingredients were injected into a Vydac C18 (Grace, USA) column (250 × 4.6 mm) and eluted in a gradient of 0–50% (v/v) acetonitrile in the presence of 0.1% (v/v) trifluoroacetic acid for 50 min for further purification. Fractions were simultaneously monitored by UV detection at 214 nm. All the chromatography separation procedures were performed at room temperature. The protein concentration in the preparations was determined by the Bradford assay.

2.2.3. Mass spectrometry analysis of CcGRN-1

Matrix-assisted laser desorption ionization time-of-flight mass spectrometry (MALDI-TOF MS) analysis was performed on an Ultraflex MALDI-TOF mass spectrometer (Bruker Daltonics, Billerica, MA, USA), equipped with a 50 Hz pulsed nitrogen laser ($\lambda = 337$ nm) and operated in positive ion reflectron mode at a 25 KV accelerating voltage. The samples were prepared by mixing an equal volume (1 μl) of peptide solution with a 1 μl matrix (α-cyano-4-hydroxycinnamicacid) saturated solution in 0.1% TFA containing 50% ACN.

2.3. Identification of CcGRN-1

2.3.1. N-terminal sequence analysis of CcGRN-1

The purified peptide was subjected to Edman degradation and analyzed by an automatic protein sequencer (ABI491, Perkin Elmer-Applied Biosystems) using standard protocols.

2.3.2. Reduction and alkylation of CcGRN-1

A freeze-dried sample (300 μg) in 150 μl of 1 M Tris–HCl buffer (pH 8.5; 6 M guanidinium hydrochloride; 0.01 M EDTA) was added to 33 μl dithiothreitol (100 mg/ml) in the same buffer and incubated at 37 °C for 8 h. Then, the sample was added with 8.7 mg iodoacetamide (IAM), and the reaction was maintained in a dark place. Two hours later, 1 ml of 0.1% TFA solution was added, and the sample was

centrifuged at 10,000 ×*g* for 5 min. The supernatant was isolated by HPLC with an MZ-ANALYTICAL C8 column in a gradient of acetonitrile in water (0.1% trifluoroacetic acid) from 0 to 40% for 40 min. The single peak eluent was analyzed by MALDI-TOF-MS.

2.3.3. Trypsin digestion of *Cc*GRN-1

The derivate sample in 600 μl of 50 mM Tris–HCl (pH 8.5) was added with 10 μl trypsin solution (0.1 mg/ml) in the same buffer. The solution was incubated for 3 h at 37 °C and separated on a Vydac C18 column using a gradient of acetonitrile in water (0.1% trifluoroacetic acid) from 0% to 40% for 40 min.

2.3.4. C-terminal sequence analysis of *Cc*GRN-1

The C-terminal peptide fragment was dissolved in 0.01 M NH_4Ac-HAc buffer (pH 6.8) and mixed with carboxypeptidase Y solution (0.1 unit) at room temperature. The reaction was stopped at different time intervals (10 s, 30 s, 1 min, 2 min, 4 min, 8 min, 16 min, 30 min, 1 h, 2 h, 5 h and 24 h) by mixing a 1 μl stop solution (saturated CCA solution in 35% acetonitrile water solution containing 0.1% TFA) and a 1 μl reaction mixture. Each reaction fraction was analyzed by MALDI-TOF-MS.

2.3.5. Bioinformatics analysis and *Cc*GRN-1 alignments

Bioinformatics analysis and alignments were performed as previously described [23]. First, the entire *Cc*GRN-1 sequence was annotated using an ExPASy software such as ProtParam. The molecular mass, isoelectric point (pI) and amino acid composition were determined using the ProtParam tool (http://www.expasy.ch/cgi-bin/protparam). The hydrophilic-hydrophobic property was analyzed using a ProtScale tool (http://www.expasy.ch/tools/protscale.html). Subcellular localization was performed using the PROST program (http://psort.hgc.jp/form.html). The signal peptide was predicted using the SignalP 4.1 Server (http://www.cbs.dtu.dk/services/SignalP/). The glycosylation and phosphorylation sites were predicted by YinOYang 1.2 (http://www.cbs.dtu.dk/services/YinOYang/) and NetPhos2.0 (http://www.cbs.dtu.dk/services/NetPhos/), respectively. The motif was analyzed in http://prosite.expasy.org/. The structural domain was analyzed in http://www.ncbi.nlm.nih.gov/Structure/cdd/cdd_help.shtml#CDUpdate. Secondary structure modeling was predicted using GOR4 (http://npsa-pbil.ibcp.fr/cgi-bin/npsa_automat.npsa_gor4.html). Second, sequence alignments were performed using the ClustalW2 program (http://www.ebi.ac.uk/Tools/msa/clustalw2/). Conserved domains were analyzed using the InterProScan and CDD websites. A phylogenetic tree

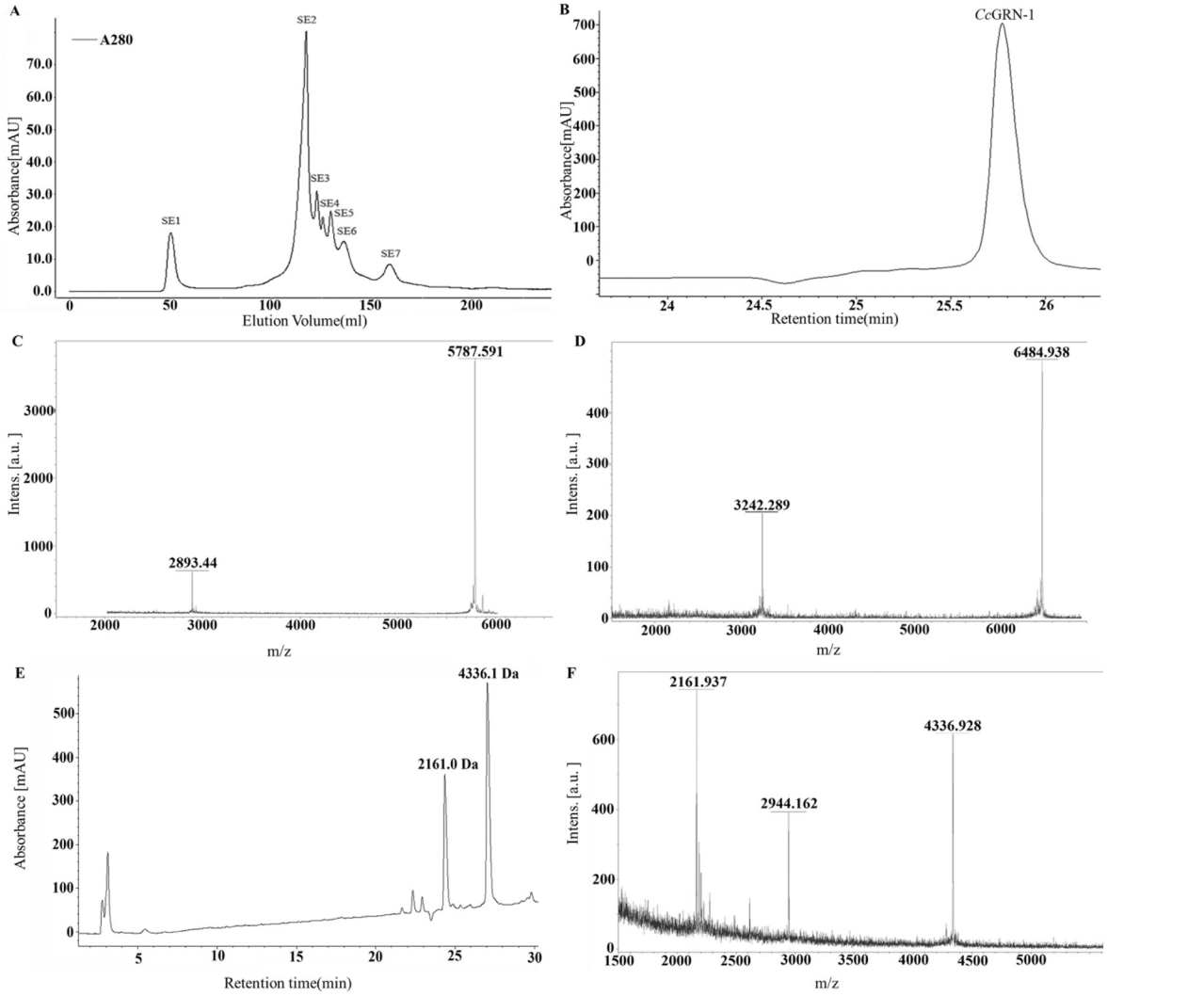

Fig. 1. Isolation and purification of *Cc*GRN-1 from rpTE and MALDI-TOF mass spectrometry of purified *Cc*GRN-1 and the *S*-carbamidomethyl derivative of *Cc*GRN-1 (S-CAM-*Cc*GRN-1). **A** rpTE was separated on a Superdex 30 column (GE Healthcare, USA) in 50 mM acetic acid at a flow rate of 1 ml/min. **B** Final reverse-phase HPLC separation of *Cc*GRN-1 occurred on a Vydac C18 (Grace, USA) column (250 × 4.6 mm) in a gradient of 0–50% (v/v) acetonitrile in the presence of 0.1% (v/v) trifluoroacetic acid for 50 min at a flow rate of 1 ml/min. **C** The monoisotopic molecular mass of *Cc*GRN-1 was determined to be 5782.92 Da. **D** The monoisotopic molecular mass of S-CAM-*Cc*GRN-1 was determined to be 6478.68 Da. **E** Reversed-phase chromatography of S-CAM-*Cc*GRN-1 trypsin hydrolysates. Two fragments were obtained (2160.9 Da and 4335.9 Da). **F** S-CAM-*Cc*GRN-1 trypsin hydrolysates were analyzed by MALDI-TOF mass spectrometry. (*m/z*: mass-to-charge ratio; a. u.: arbitrary units).

Table 1
Identification of the amino acid sequence of *Cc*GRN-1.

Sequence 1	NVICPDGTSFCASGQTCCK**LSSGSYGCCPL**
Sequence 2	**LSSGSYGCCPL**PNAVCCSDGVHCCPSGTTCDVSQG
Sequence 3	NVICPDGTSFCASGQTCCKLSSGSYGCCPLPNAVCCSDGVHCCPSGTTCDVSQG
Sequence 4	QGTCL(I) *R
Sequence 5	NVICPDGTSFCASGQTCCKLSSGSYGCCPLPNAVCCSDGVHCCPSGTTCDVSQGTCL(I)*R

was further established using MEGA 4 software to analyze the relationship between *Cc*GRN-1 and its homologous molecules in different species. Finally, functional and metabolic pathways were analyzed using the Kyoto Encyclopedia of Genes and Genomes (KEGG) pathway database (http://www.genome.jp/kegg) to obtain functional annotations and analyze biological processes involved in metabolism.

2.4. Cell culture and cell viability assay

Human umbilical vein endothelial cells (HUVECs) (Zhongqiao Xinzhou Biotech, Shanghai, China) were grown in high-glucose DMEM medium (HyClone, Waltham, MA, USA) supplemented with 10% fetal calf serum (FBS, Gibco, USA), 100 U/ml penicillin, and 100 μg/ml streptomycin at 37 °C in a humidified incubator with 95% air and 5% CO_2.

Cell viability was determined by the CCK-8 assay. The HUVECs were plated in 96-well culture plates at a density of 1×10^4 cells/ml. After incubation for 24 h, the cells were treated with *Cc*GRN-1 (0–32 μg/ml) for 12 h, 24 h and 48 h. Then, 10 μl of CCK-8 reagents was added to each well for 4 h at 37 °C. Absorbance at 450 nm was measured using a microplate reader (BioTek, Winooski, VT, USA). Cell-growth frequency was calculated using the following formula:

$$\text{Proliferation}\ (\%) = (1-\text{OD}_{\text{treated}}/\text{OD}_{\text{untreated}}) \times 100.$$

2.5. Cell-cycle analysis

The HUVECs, seeded in 6-well culture plates (3×10^5 cells/well), were treated with *Cc*GRN-1 (0.5 μg/ml) for different time durations (0–360 min). Then, the trypsin-harvested cells were fixed in ice-cold 75% ethanol at 4 °C for 30 min. The cells were washed twice with PBS at room temperature then incubated with a staining solution containing PI (50 μg/ml) and Rnase A (50 μg/ml) for 30 min. The fluorescence was measured and analyzed using an FAC Scan flow cytometer (Becton Dickinson, San Jose, CA, USA).

2.6. Western blotting

To investigate the *Cc*GRN-1 effect on the cell-cycle protein expression, the HUVECs were treated with *Cc*GRN-1 (0.5 μg/ml) for different time durations (0–360 min). To explore the *Cc*GRN-1 effect on signaling-protein phosphorylation, the HUVECs were treated with *Cc*GRN-1 (0.5 μg/ml) for different time durations (0–60 min) in the presence or absence of LY294002 (10 μM), PD98059 (10 μM), SP600125 (10 μM) and Bay11-7082 (10 μM). To survey the effect of signaling-pathway inhibitors on the expression of *Cc*GRN-1-induced cell-cycle proteins, the HUVECs were pretreated with *Cc*GRN-1 (0.5 μg/ml) for 30 min in the presence or absence of LY294002 (10 μM) or PD98059 (10 μM).

After treatments, the cells were lysed on ice in an RIPA buffer with a protease inhibitor (1% PMSF). The protein content was measured by the Bradford assay. Equal amounts of protein per sample were loaded on a 12% SDS-PAGE gel and transferred to a polyvinylidene difluoride or nitrocellulose membrane, which was then blocked with 5% non-fat dry milk in TBST (3 g Tris-base, 8 g NaCl, 0.2 g KCl, 0.05% Tween-20, diluted with water to 1000 ml, pH 7.4) for 2 h at room temperature. The membranes were then incubated overnight at 4 °C with primary antibodies as follows: p-Akt (1: 1000), Akt (1: 1000), p-ERK1/2 (1: 1000), ERK1/2 (1: 1000), p-JNK (1: 500), JNK (1: 500), p-NF-κB (1: 1000), NF-κB (1: 1000), p-IκBα (1: 500), CyclinB1 (1: 1000), CyclinD1 (1: 1000), GAPDH (1: 5000) and beta-Tubulin (1: 1000), with gentle shaking. The electrochemiluminescence method was used with secondary antibodies (HRP-conjugated anti-rabbit IgG and anti-mouse IgG) at a dilution of 1: 5000 for 2 h at room temperature. Afterward, the membranes were exposed using a chemiluminescent detection system (Syngene G: Box, USA). Quantitative densitometric analyses of immunoblots were performed using ImageJ software (Ver. 1.48, Bethesda, MD, USA), and the relative ratio was calculated.

2.7. Immunofluorescence staining

The HUVECs were grown on coverslips located in 6-well culture plates. The control group was incubated with PBS, and other groups were incubated with *Cc*GRN-1 (0.5 μg/ml) in the presence or absence of LY294002, PD98059 or SP600125. Then, the HUVECs were fixed with a 4% paraformaldehyde solution for 30 min and permeabilized with a 0.5% Triton X-100 solution (in PBS) for 5 min at room temperature. Subsequently, the HUVECs were blocked with 5% BSA (in PBS) for 30 min at room temperature and incubated overnight at 4 °C with primary antibodies as follows: p-Akt (1: 100), p-ERK1/2 (1: 100), p-JNK (1: 100), CyclinB1 and CyclinD1 (1: 200). After incubation with the primary antibodies, the HUVECs were further incubated with FITC-labeled goat anti-rabbit or anti-mouse antibodies for 3 h and incubated with DAPI (10 μg/ml) for 1 min at room temperature. Afterward, coverslips were sealed onto the slides with an antifade mountant. Finally, fluorescence images were visualized using a confocal laser-scanning microscope (Olympus FV 1000, Japan) with excitation and emission wave lengths of 492 nm and 520 nm, respectively. Fluorescence intensities were obtained from the image dataset using FV10-ASW 3.1 software (Olympus FV 1000, Japan).

Table 2
C-terminal sequence analysis of 4336.1 Da peptide.

Peptide number	Observed fragment mass[*m*/*z*]	Deduced sequence
1	2397.073	LSSGSYGCCPLPNAVCCSDGVH
2	2557.122	LSSGSYGCCPLPNAVCCSDGVHC
3	2797.978	LSSGSYGCCPLPNAVCCSDGVHCCP
4	2901.099	LSSGSYGCCPLPNAVCCSDGVHCCPS
5	3059.316	LSSGSYGCCPLPNAVCCSDGVHCCPSGT
6	3160.508	LSSGSYGCCPLPNAVCCSDGVHCCPSGTT
7	3320.541	LSSGSYGCCPLPNAVCCSDGVHCCPSGTTC
8	3435.586	LSSGSYGCCPLPNAVCCSDGVHCCPSGTTCD
9	3621.889	LSSGSYGCCPLPNAVCCSDGVHCCPSGTTCDVS
10	3749.499	LSSGSYGCCPLPNAVCCSDGVHCCPSGTTCDVSQ
11	3806.680	LSSGSYGCCPLPNAVCCSDGVHCCPSGTTCDVSQG
12	3907.763	LSSGSYGCCPLPNAVCCSDGVHCCPSGTTCDVSQG**T**
13	4067.601	LSSGSYGCCPLPNAVCCSDGVHCCPSGTTCDVSQG**TC**
14	4180.783	LSSGSYGCCPLPNAVCCSDGVHCCPSGTTCDVSQGTC**L(I)** *
15	4336.870	LSSGSYGCCPLPNAVCCSDGVHCCPSGTTCDVSQGTCL(I) ***R**

2.8. Migration assay

Cell migration was studied using the wound healing scratched assay and the transwell assay. For the wound healing scratched assay, HUVECs were seeded in 6-well culture plates (3×10^5 cells/well) and grown to confluence. After serum starvation, the cells were scraped to create a wound area in the centers of the cell monolayers (time point set as 0 h). Then, the cells were washed with PBS and incubated with *Cc*GRN-1 (0.5 μg/ml) in the presence or absence of PD98059 (20 μM) or with PD98059 (20 μM) directly for 24 h. The wound closure was photographed at different time durations (0, 12, 24 h) at 100×. The extent of wound closure was quantitated by calculating the difference in the denuded area using ImageJ software. For the transwell assay, chambers with 8-μm polyester filters were used (Corning, Corning, NY, USA). HUVECs (200 μl, 1×10^4 cells/ml) were placed in the upper compartment in serum-free medium and treated with *Cc*GRN-1 (0.5 μg/ml) in the presence or absence of PD98059 (20 μM) or with PD98059 (20 μM) directly. The lower chambers, which were devoid of cells, were filled with DMEM (500 μl) with 10% fetal bovine serum and placed in 24-well plates. After different incubation durations (6, 12, 24 h) incubation, the cells on the lower surface of the chamber were fixed with 4% paraformaldehyde and stained with crystal violet for 20 min. Five visual fields were randomly selected from each Transwell filter and captured at 400× magnification using an inverted fluorescence microscope (Nikon Eclipse Ti-S). The average number of cells that migrated through the Transwell filter was assayed using ImageJ software.

2.9. Statistical analysis

In the experiments, the images shown were the representatives of at least three experiments performed on different experimental days. Data were presented as the mean ± SEM. Analysis of variance (One-way ANOVA) and Bonferroni's *post hoc* test were used to statistically evaluate the data when appropriate. A value of $P < 0.05$ was considered statistically significant.

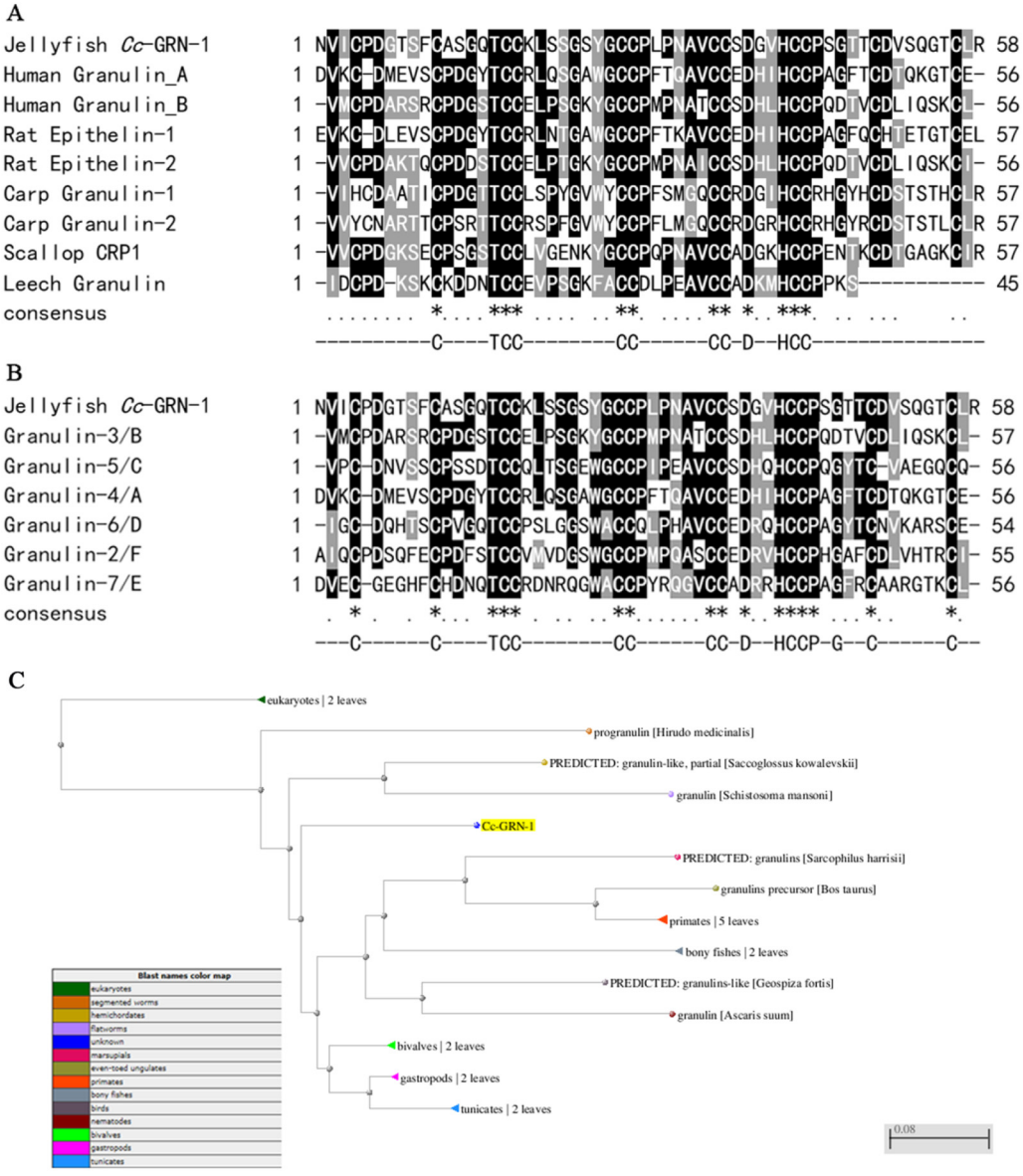

Fig. 2. Multiple sequence alignment and phylogenetic analysis of *Cc*GRN-1. A Multiple sequence alignment of *Cc*GRN-1 amino acid sequence with other eukaryotic granulin sequences. B Multiple sequence alignment of *Cc*GRN-1 amino acid sequence with human granulin sequences. C Phylogenetic analysis of the amino acid sequence of *Cc*GRN-1 compared with other known granulins. Completely conserved residues across all aligned sequences are shaded in black and marked below with an asterisk (*). Highly conserved residues are indicated by dots (.) and shaded in gray. Absent amino acids are indicated by dashes (−).

3. Results

3.1. Isolation and purification of CcGRN-1 from rpTE

The rpTE was fractionated on a Superdex 30 column, as shown in Fig. 1A. Each fraction was subsequently analyzed by MALDI-TOF-MS, and the fractions containing peptide with a molecular weight of approximately 5800 Da were pooled and further purified by reverse-phase HPLC. After 2 HPLC purification steps, a pure peptide was obtained (Fig. 1B).

The molecular weight of isolated peptide *Cc*GRN-1 was determined by MALDI-TOF MS. Since the mass spectrometer resolution at *m*/*z* 5800 was not sufficiently high to present the monoisotopic peak, the monoisotopic molecular weight was calculated from the m/z 2892.46 double-charged ions, where the resolution was much better. The monoisotopic molecular weight of *Cc*GRN-1 was 2892.46 × 2–2 = 5782.92 Da (Fig. 1C). In the same way, the monoisotopic molecular weight of the reductive alkylation product of *Cc*GRN-1 was 3240.34 × 2–2 = 6478.68 Da (Fig. 1D). A mass change of 696 Da resulted when comparing the MALDI-TOF mass spectra of *Cc*GRN-1 before and after the reductive alkylation, indicating that the 12 Cys residues in *Cc*GRN-1 form 6 disulfide bonds in the natural peptide.

3.2. Identification of CcGRN-1 amino acid sequence

The reductive alkylation product *Cc*GRN-1 was subjected to an automatic protein sequencer to determine the N-terminal sequence. In the first try, 30 amino acid residues were observed as Sequence 1 (Table 1). After trypsin hydrolysis, two fragments were obtained by purification with reverse-phase HPLC (Fig. 1E). The fragment with a molecular weight 2160.9 Da consists of 19 N-terminal amino acids according to the molecular weight calculation, and the other one (4335.9 Da) corresponds to the C-terminal region (Fig. 1F). Automatic sequencing of the C-terminal fragment revealed 35 amino acid residues as Sequence 2 (Table 1), of which 11 overlap with the N-terminal fragment. Thus, the *Cc*GRN-1 sequence was deduced as Sequence 3 (54 residues) (Table 1). However, several residues in the C-terminus remain unknown. Therefore, carboxypeptidase Y was used to determine the C-terminal sequence. The peptide fragments obtained after carboxypeptidase Y hydrolysis were listed subsequently in Table 2, clearly revealing the 6 residues from C terminus as Sequence 4 (Table 1). At this point, the residue with a molecular weight 113 Da could be either Leucine or Isoleucine.

These results showed that *Cc*GRN-1 has 58 amino acids, and its complete sequence is as shown in Sequence 5 (Table 1), which includes 12 cysteine residues forming 6 disulfide bonds. The observed monoisotopic molecular weight of this sequence is identified using the calculated one, 5782.24 Da. Homologic analysis showed that this sequence was highly similar to members of the granulin family. Therefore, the peptide was named *Cyanea capillata* granulin-1 (*Cc*GRN-1). A sequential comparison using ClustalW analysis revealed conservation of several repetitions of cysteine-rich structures between *Cc*GRN-1 and other granulin amino acid sequences (Fig. 2A). Similarly, the jellyfish *Cc*GRN-1 sequence exhibited a high structural conservation with human granulin sequences (Fig. 2B). Moreover, phylogenetic analyses revealed that jellyfish *Cc*GRN-1 clustered with the bivalve granulins, suggesting its close resemblance to the Cnidarian counterpart. The other bioinformatics analysis results can be found in the Supplementary data (Supplementary Figs. S1, S2 and S3).

Table 1 Amino acid sequence of CcGRN-1 was identified. N-terminal 30 amino acid residues were observed as Sequence 1. The C-terminal fragment revealed 35 amino acid residues as Sequence 2, in which 11 overlapping residues were shown in bold, and the sequence was deduced to be Sequence 3 (54 residues). The terminal 6 residues from C terminus were identified as Sequence 4. The complete 58 amino acid sequence was shown as Sequence 5. L(I) *: the residue could be either Leucine or Isoleucine.

Table 2 C-terminal fragments obtained after carboxypeptidase Y hydrolysis were listed. The terminal 4 residues were shown in bold. L(I)*: the residue with a molecular weight 113 Da could be either Leucine or Isoleucine.

3.3. Effects of CcGRN-1 on HUVEC viability

As shown in Fig. 3, HUVEC viability was increased in a dose- and time-dependent manner after treatment with *Cc*GRN-1, which demonstrated that *Cc*GRN-1 could effectively promote cell proliferation.

3.4. Effects of CcGRN-1 on the cell cycle of HUVECs

3.4.1. Effects of CcGRN-1 on the cycle progression of HUVECs

To further elucidate the proliferation-promoting mechanism of *Cc*GRN-1, *Cc*GRN-1 effects on cell-cycle progression were examined by flow cytometry. As shown in Fig. 4A, *Cc*GRN-1 (0.5 μg/ml) induced the transition of cells from the G1-phase to the S/G2-phase in a time-dependent manner. The cell-cycle analysis showed a significant cell decrease from 66.87% to 58.72% in the G1-phase and an increase from 33.13% to 41.28% in the S/G2-phase (Fig. 4B). These results indicated that *Cc*GRN-1 might promote HUVEC transition from the G1- to the S/G2-phase, ultimately promoting cell proliferation.

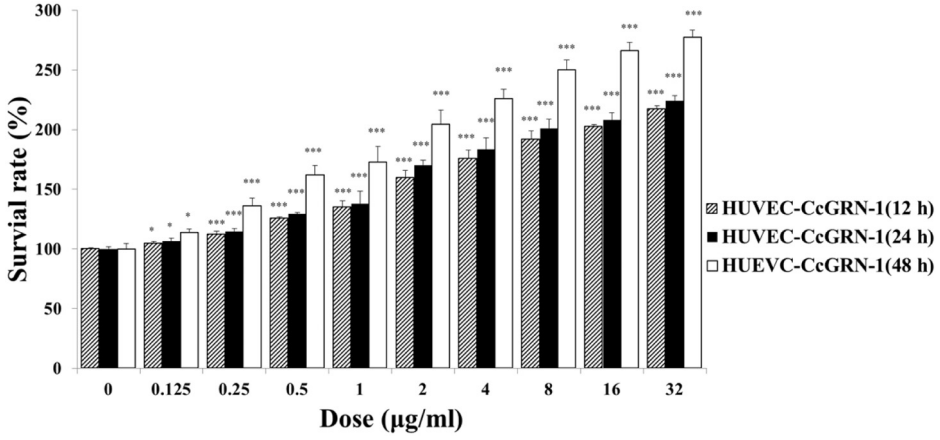

Fig. 3. *Cc*GRN-1 effects on HUVEC viability. The HUVECs were stimulated with different doses of *Cc*GRN-1 (0–32 μg/ml) for 12 h, 24 h and 48 h. HUVEC viability was measured by the CCK-8 assay. $^{\triangle}P < 0.05$, $^{\triangle\triangle\triangle}P < 0.001$ *vs.* Control (12*h*), $^{***}P < 0.001$ *vs.* Control (24 h), $^{\#}P < 0.05$, $^{\#\#\#}P < 0.001$ *vs.* Control (48 h).

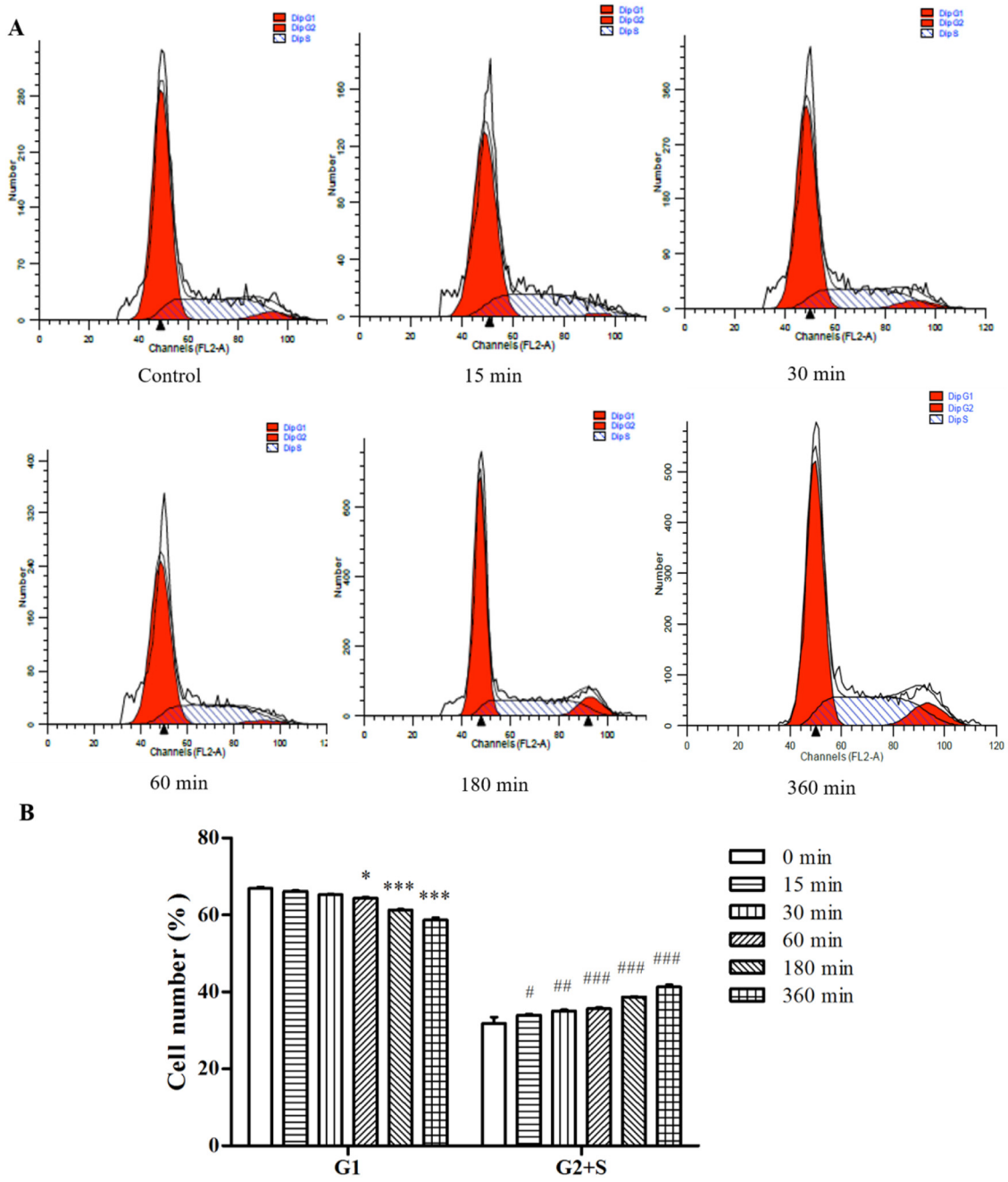

Fig. 4. Effects of *Cc*GRN-1 on HUVEC cycle progression. **A** Representative histograms showing cell-cycle distribution upon *Cc*GRN-1 (0.5 μg/ml) for different times. **B** Bar graph summarizing cell-cycle data. $^{*}P < 0.05$, $^{***}P < 0.001$ *vs.* Control of G1-phase. $^{\#}P < 0.05$, $^{\#\#}P < 0.01$, $^{\#\#\#}P < 0.001$ *vs.* Control of S/G2-phase.

3.4.2. Effects of CcGRN-1 on the cell-cycle protein expression of HUVECs

As shown in Fig. 5, CyclinB1 expression increased significantly from 30 to 60 min after *Cc*GRN-1 (0.5 μg/ml) treatment, with the maximal expression occurring at approximately 30 min. Similarly, the expression of CyclinD1 was induced with *Cc*GRN-1, with the maximum expression occurring at approximately 30 min. These results indicated that *Cc*GRN-1 could activate the expression of cell-cycle proteins.

3.5. Effects of CcGRN-1 on the cell signaling pathways in HUVECs

3.5.1. Effects of CcGRN-1 on the cell signaling pathways in HUVECs by western blotting

As shown in Fig. 6A, Akt phosphorylation was markedly induced by *Cc*GRN-1 (0.5 μg/ml) from 5 to 30 min, with the maximal phosphorylation occurring at approximately 15 min, while *Cc*GRN-1 seemed to have no effect on the total Akt level. On the other hand, we pretreated the HUVECs with the PI3K-, ERK1/2–, JNK MARK– or NF-κB-signaling inhibitors before *Cc*GRN-1 presence to confirm whether the PI3K/Akt-signaling pathway was involved. The PI3K inhibitor LY294002 completely blocked *Cc*GRN-1-induced Akt phosphorylation, while other signaling-pathway inhibitors—including PD98059, SP600125 and Bay11–7082—had no effect (Fig. 6B). These results indicated that *Cc*GRN-1 could activate the PI3K/Akt-signaling pathway.

As shown in Fig. 6C, ERK1/2 phosphorylation was markedly induced using *Cc*GRN-1 (0.5 μg/ml) from 15 to 30 min, with the maximal phosphorylation occurring at approximately 15 min, while *Cc*GRN-1 seemed to have no effect on the level of total ERK1/2. Then, we pretreated the HUVECs with the PI3K-, ERK1/2–, JNK MARK– or NF-κB-signaling inhibitors before *Cc*GRN-1 presence to confirm whether the ERK1/2 MARK–

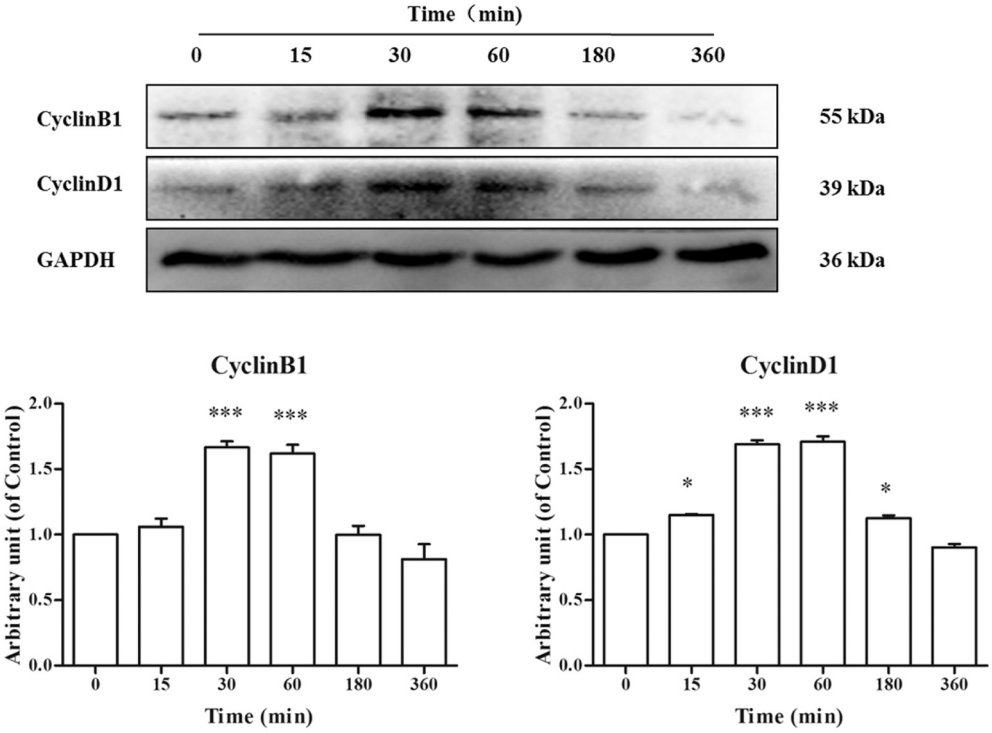

Fig. 5. Effects of *Cc*GRN-1 on the expression of cell-cycle proteins (CyclinB1 and CyclinD1) in HUVECs. $^{*}P < 0.05$, $^{***}P < 0.001$ *vs.* Control.

signaling pathway was involved. The ERK 1/2 MAPK inhibitor PD98059 completely blocked *Cc*GRN-1-induced ERK1/2 phosphorylation, while other signaling-pathway inhibitors—including LY294002, SP600125 and Bay11-7082—had no effect (Fig. 6D). These results indicated that *Cc*GRN-1 could activate the ERK1/2 MAPK–signaling pathway.

However, *Cc*GRN-1 (0.5 μg/ml) seemed to have no effect on the level of p-JNK, p-NF-κB and p-IκBα, which indicated that *Cc*GRN-1 could not activate the JNK MAPK– and the NF-κB-signaling pathway (Supplementary Fig. S4 and S5).

3.5.2. Effects of CcGRN-1 on the cell signaling pathways in HUVECs by immunofluorescence

To further explore the effects of *Cc*GRN-1 upon PI3K/Akt-, ERK1/2- and JNK-signaling pathways, the HUVECs were analyzed by immunofluorescence staining with corresponding antibodies (green) in the presence or absence of respective inhibitors. DNA staining with DAPI (blue) was used to define nuclei.

As shown in Fig. 7, *Cc*GRN-1 (0.5 μg/ml) could markedly induce Akt phosphorylation, while LY29400 completely blocked *Cc*GRN-1-induced Akt phosphorylation. Similarly, ERK1/2 phosphorylation was significantly induced by *Cc*GRN-1 (0.5 μg/ml), while PD98059 completely blocked *Cc*GRN-1-induced ERK1/2 phosphorylation. On the other hand, *Cc*GRN-1 had no effect on the p-JNK level. These results further confirmed that *Cc*GRN-1 could activate PI3K/Akt- and ERK1/2 MAPK–signaling pathways but not the JNK MAPK–signaling pathway.

3.6. Effects of signaling-pathway inhibitors on the expression of CcGRN-1-induced cell-cycle proteins in HUVECs

3.6.1. Effects of signaling-pathway inhibitors on the expression of CcGRN-1-induced cell-cycle proteins in HUVECs by western blotting

Since *Cc*GRN-1 (0.5 μg/ml) could activate PI3K/Akt- and ERK1/2 MAPK–signaling pathways, corresponding pathway inhibitors were selected to investigate their roles in the *Cc*GRN-1-induced expression of cell-cycle proteins.

As shown in Fig. 8, the *Cc*GRN-1-induced expression of CyclinB1 and CyclinD1 was blocked with PD98059 but not LY294002, which demonstrated that the ERK1/2 MAPK–signaling pathway was involved in *Cc*GRN-1-induced cell-cycle protein expression in HUVECs.

3.6.2. Effects of pathway inhibitors on the expression of CcGRN-1-induced cell-cycle proteins in HUVECs by immunofluorescence

As shown in Fig. 9, *Cc*GRN-1 (0.5 μg/ml) increased CyclinB1 and CyclinD1 expression. However, the effect was markedly blocked by the PD98059 pretreatment but not affected by LY294002, which further confirmed that the ERK1/2 MAPK–signaling pathway was involved in TE-induced cell-cycle protein expression in HUVECs.

3.7. Effect of CcGRN-1 on wound healing

Since the ERK1/2 MAPK–signaling pathway was involved in the *Cc*GRN-1-induced cell-cycle protein expression, we further investigated whether *Cc*GRN-1 affected cell migration in the presence or absence of the ERK1/2 MAPK inhibitor by the wound healing and the transwell assay, respectively.

As shown in Fig. 10A, B, the results of the wound healing assay indicated that *Cc*GRN-1 (0.5 μg/ml) markedly induced cell migration in a time-dependent manner. The relative migration was approximately 129% at 12 h and 163% at 24 h. However, the *Cc*GRN-1-induced cell migration could be markedly attenuated by PD98059. Similarly, the results of the transwell assay showed that the number of migrating cells increased at 12 h and 24 h when HUVECs were treated with *Cc*GRN-1 (0.5 μg/ml) and the *Cc*GRN-1-induced cell migration could also be attenuated by PD98059 (Fig. 10C, D). These results demonstrated that the ERK1/2 MAPK–signaling pathway was involved in *Cc*GRN-1-induced endothelial cell migration.

4. Discussion

Wound healing is a complex and coordinated multicellular process. First, the wound is sealed by clotting and soon infiltrated by inflammatory cells. Next, keratinocytes divide and migrate to reestablish the epidermal layer—namely, reepithelialization—and then, fibroblast and endothelia from the wound margins divide and enter the wound,

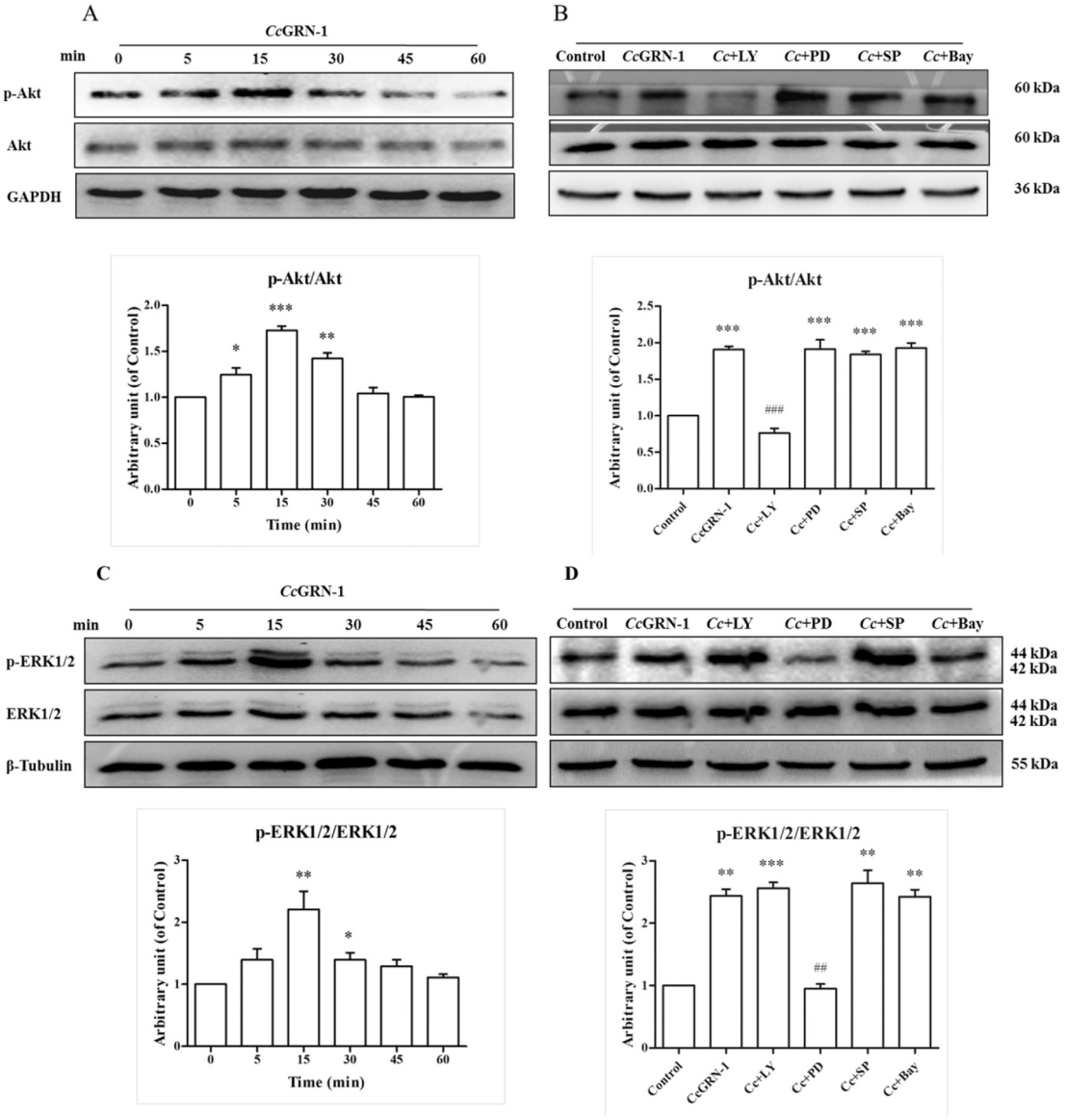

Fig. 6. Responses of the PI3K/Akt- and the ERK1/2 MAPK–signaling pathway to *Cc*GRN-1 (0.5 μg/ml). A, C HUVECs were treated with *Cc*GRN-1 (0.5 μg/ml) for various time durations. B, D HUVECs were treated with *Cc*GRN-1 (0.5 μg/ml) in the presence or absence of various signaling-pathway inhibitors for 15 min. *Cc*: *Cc*GRN-1, LY: LY294002, PD: PD98059, SP: SP600125, Bay: Bay11–7082. $^{*}P < 0.05$, $^{**}P < 0.01$, $^{***}P < 0.001$ *vs.* Control. $^{\#\#}P < 0.01$, $^{\#\#\#}P < 0.001$ *vs.* *Cc*GRN-1.

establishing the granulation tissue comprising fibroblasts and new blood vessels. At later stages, matrix deposition and wound contraction [24–26] occur. During these processes, multiple growth factors and cytokines are readily present in the wound bed and play a role in all stages of wound healing. Numerous studies have shown that the activation of EGFR increases the migration and proliferation of keratinocytes and accelerates wound reepithelialization, FGF and VEGF participate in granulation tissue formation and stimulate angiogenes, and PDGF plays a role in each stage of wound healing [2,5,27,28]. For this reason, several studies have been performed on the effect of topically applied recombinant growth factors in experimental wound healing or randomized controlled clinical trials [2,3]. However, past attempts through topical application of growth factors to refractory ulcers have not been efficacious. For instance, a phase I clinical trial for topical recombinant human VEGF (rhVEGF) showed no significant therapeutic benefit in chronic diabetic foot ulcers [7]. In another study, FGF-2 was topically applied daily to 17 patients with diabetic foot ulcers in a double-blinded, randomized manner, but no significant difference was observed [29]. The possible reason is that recombinant growth factors suffer from some side effects such as susceptibility to proteases and rapid plasma clearance [2,7,8]. Due to these limitations, purification and identification of novel growth factors for wound healing is still in progress.

Marine-derived bioactive components such as pyranone [30], polysaccharide [31,32], anthraquinone [33] and collagen-derived peptides [34] have long been used as a vital source of drug candidates that promote and accelerate the wound healing process. Besides, numerous

Fig. 7. Effects of *Cc*GRN-1 (0.5 μg/ml) on signaling-pathway phosphorylation in the presence or absence of inhibitors. **A** HUVECs were pretreated with *Cc*GRN-1 (0.5 μg/ml) for 15 min in the presence or absence of an inhibitor for the PI3K/Akt-signaling pathway. **B** HUVECs were pretreated with *Cc*GRN-1 (0.5 μg/ml) for 15 min in the presence or absence of an inhibitor for the ERK1/2 MAPK–signaling pathway. **C** HUVECs were pretreated with *Cc*GRN-1 (0.5 μg/ml) for 15 min in the presence or absence of an inhibitor for the JNK MAPK–signaling pathway. Images were obtained by a fluorescence microscope at 600 × magnification, scale = 30 μm. *Cc*: *Cc*GRN-1, LY: LY294002, PD: PD98059, SP: SP600125. $^{***}P < 0.001$ *vs.* Control. $^{\#\#\#}P < 0.001$ *vs.* *Cc*GRN-1.

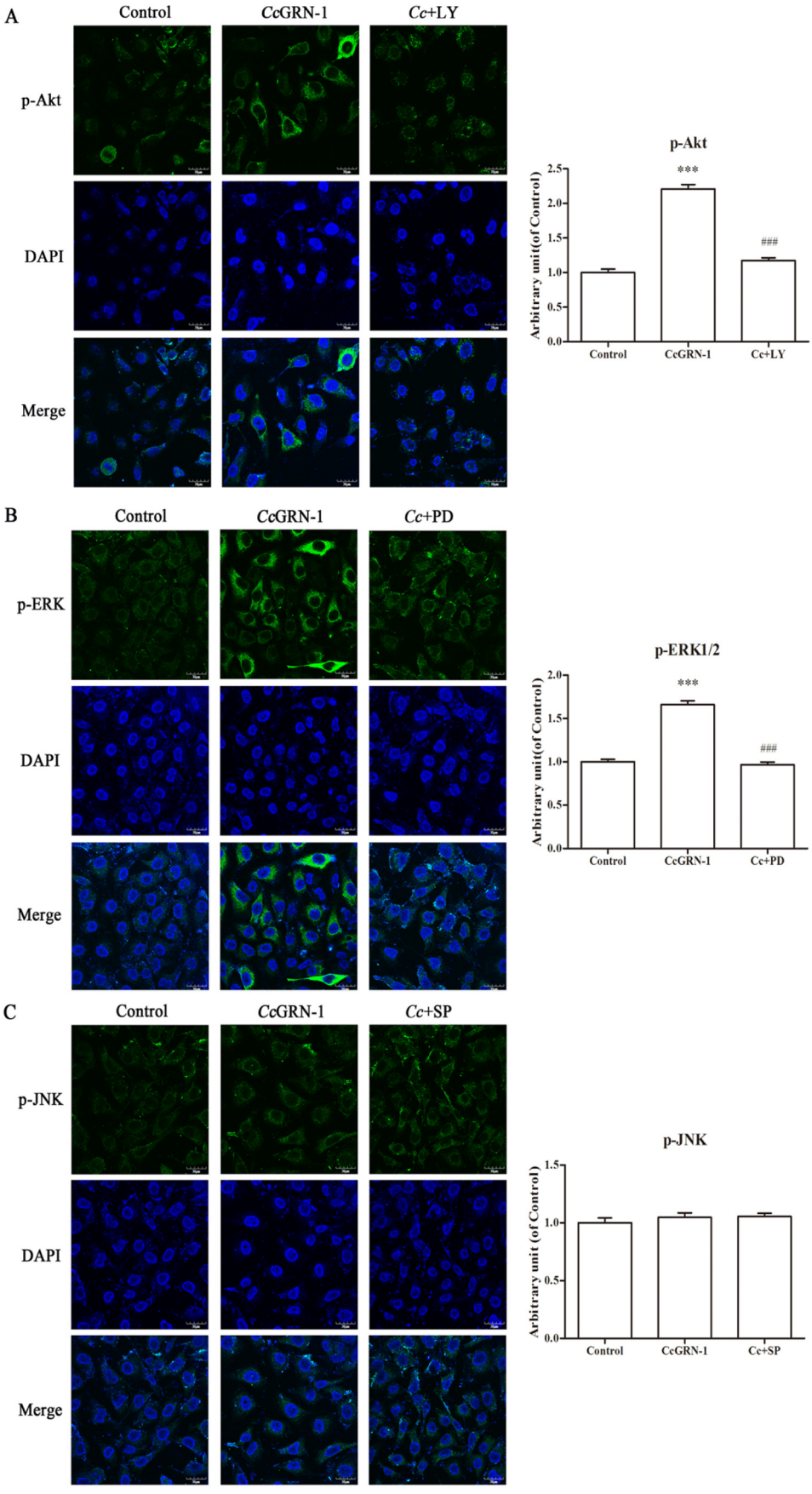
A
Control
CcGRN-1
Cc+LY
p-Akt
DAPI
Merge
p-Akt
***
###
Arbitrary unit(of Control)
2.5
2.0
1.5
1.0
0.5
0.0
Control
CcGRN-1
Cc+LY
B
Control
CcGRN-1
Cc+PD
p-ERK
DAPI
Merge
p-ERK1/2
***
###
Arbitrary unit(of Control)
2.0
1.5
1.0
0.5
0.0
Control
CcGRN-1
Cc+PD
C
Control
CcGRN-1
Cc+SP
p-JNK
DAPI
Merge
p-JNK
Arbitrary unit (of Control)
1.5
1.0
0.5
0.0
Control
CcGRN-1
Cc+SP

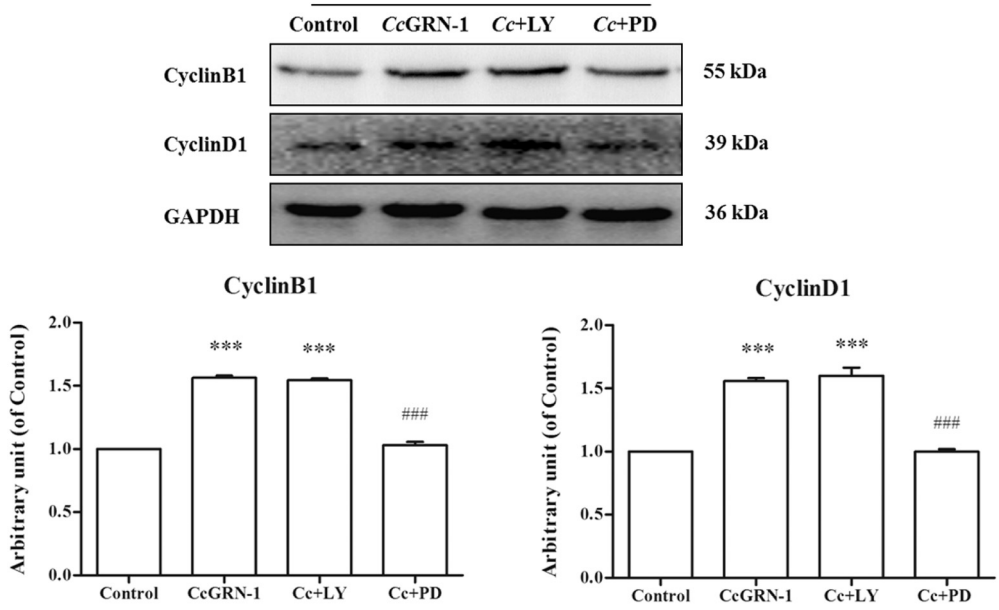

Fig. 8. Effects of signaling-pathway inhibitors on the *Cc*GRN-1-induced expression of CyclinB1 and CyclinD1. HUVECs were pretreated with *Cc*GRN-1 (0.5 μg/ml) for 30 min in the presence or absence of inhibitors of the Akt- and ERK1/2 MAPK–signaling pathways, respectively. *Cc*: *Cc*GRN-1, LY: LY294002, PD: PD98059. $^{***}P < 0.001$ *vs.* Control. $^{\#\#\#}P < 0.001$ *vs. Cc*GRN-1.

marine bioactive molecules have been isolated and developed into tissue-engineered substitutes with healing-promoting properties, such as astaxanthin incorporated collagen film [35] and chitosan hydrogel in combination with marine peptides [36].

In the present study, we successfully isolated and purified a novel polypeptide with a molecular mass of 5782 Da from the jellyfish *C. capillata* using size-exclusion chromatography followed by reverse-phase HPLC. Homologic analysis showed that this peptide belonged to the granulin (GRN) family of growth factors; thus, we named it *Cyanea capillata* granulin-1 (*Cc*GRN-1). GRNs, also known as epithelins, are a family of secreted, glycosylated peptides of approximately 6 kDa composed of a highly conserved motif of 12 cysteines and characterized by 6 disulfide bridges [37]. Sequence analysis showed that the jellyfish *Cc*GRN-1 consisted of 58 amino acids which also included 12 cysteine residues forming 6 disulfide bonds, exhibiting a high structural conservation with other GRN peptides. As a group of growth factors, GRNs have been shown to be involved in numerous physiological processes such as wound healing, cell growth and proliferation modulation [37]. In this study, we demonstrated that *Cc*GRN-1 could promote cell viability in a dose- and time-dependent manner. Then, we proved that *Cc*GRN-1 (0.5 μg/ml) could increase the expression of cell-cycle proteins (CyclinB1 and CyclinD1) and ultimately regulate cell proliferation. To our knowledge, this is the first time that GRN with growth-promoting properties was found in jellyfish. Our study will enrich the current knowledge on the role of GRN on proliferation and migration.

GRN originates from a posttranslational proteolytic processing of a larger precursor, progranulin (PGRN), a secreted growth factor that mediates cell-cycle progression and cell motility [38–40]. It has been reported that PGRN mRNA levels were upregulated for at least 10 days in murine transcutaneous puncture wounds [24,41]. In addition, when PGRN was administered to a fresh cutaneous wound, inflammation infiltration and accumulation of fibroblasts and blood vessels increased in the wound [41]. However, recombinant human PGRN could easily be hydrolyzed with elastase and chymotrypsin released during infection and inflammation, which affected PGRN's wound-healing capacity [42]. Compared with their precursor proteins, GRNs were also reported to exhibit growth-modulating activities on certain cell types. However, until now, biological functions and the underlying mechanisms of GRNs remain controversial [43–45]. Therefore, another aim of our present study was to explore the possible mechanisms by which *Cc*GRN-1 drives cell proliferation and wound repair.

Previous studies have shown that PGRN could activate typical growth-factor pathways such as the PI3K and ERK signal cascades, promote the expression of cyclin B and D, and stimulate cell proliferation and migration [46]. In this study we first examined the effect of *Cc*GRN-1 on PI3K- and MAPK-signaling pathways and found that *Cc*GRN-1 could activate PI3K/Akt and ERK1/2-signaling pathway. Consequently, we performed additional experiments to further establish the role of PI3K/Akt- and ERK1/2 signaling pathways in *Cc*GRN-1-induced proliferative effects in the HUVECs. It was showed that only the ERK1/2 MAPK–signaling pathway was involved in regulating *Cc*GRN-1-induced proliferation. In addition, wound-healing assay showed that the *Cc*GRN-1-induced cell migration ability was notably impaired by the ERK1/2 inhibitor. These results adequately demonstrated that the ERK1/2 signaling pathway regulates *Cc*GRN-1-induced endothelial cell migration, which may aid the further understanding of the mechanism of action of GRNs.

ERK1/2 signaling pathway has been reported to be involved in regulating cell migration and can be activated by various stimuli, including cytokines, transforming agents and growth factors [47]. However, little is known about how GRNs activate ERK1/2. Also, there is still limited information on GRNs structure/function relationships. It has been elucidated that GRNs characterized a novel protein architecture of four stacked β-hairpins with an axial rod of disulfide bridges, which showed some similarity with EGF in their respective tertiary structures [48]; and the precursors for mammalian granulins and EGF are both characterized as multiple repeats of conserved cysteine modules [49,50]. Although no evidence showed that granulin peptides bind EGF receptors, partial superimposition between the three-dimensional folds of granulin and the EGF family of peptides may indicate an underlying similarity in the way the peptides from these two families interact with their respective receptors. Further studies are required to obtain the structural information of *Cc*GRN-1 and determine the correlation between structure and function in promoting cell proliferation.

Besides the lack of structural information of *Cc*GRN-1, this study has several other limitations. For example, it does not provide the information about the half-life time and the characteristics of degradation of *Cc*GRN-1. Peptides delivered to the wound environment face many challenges because of their low content in the surface of wounds,

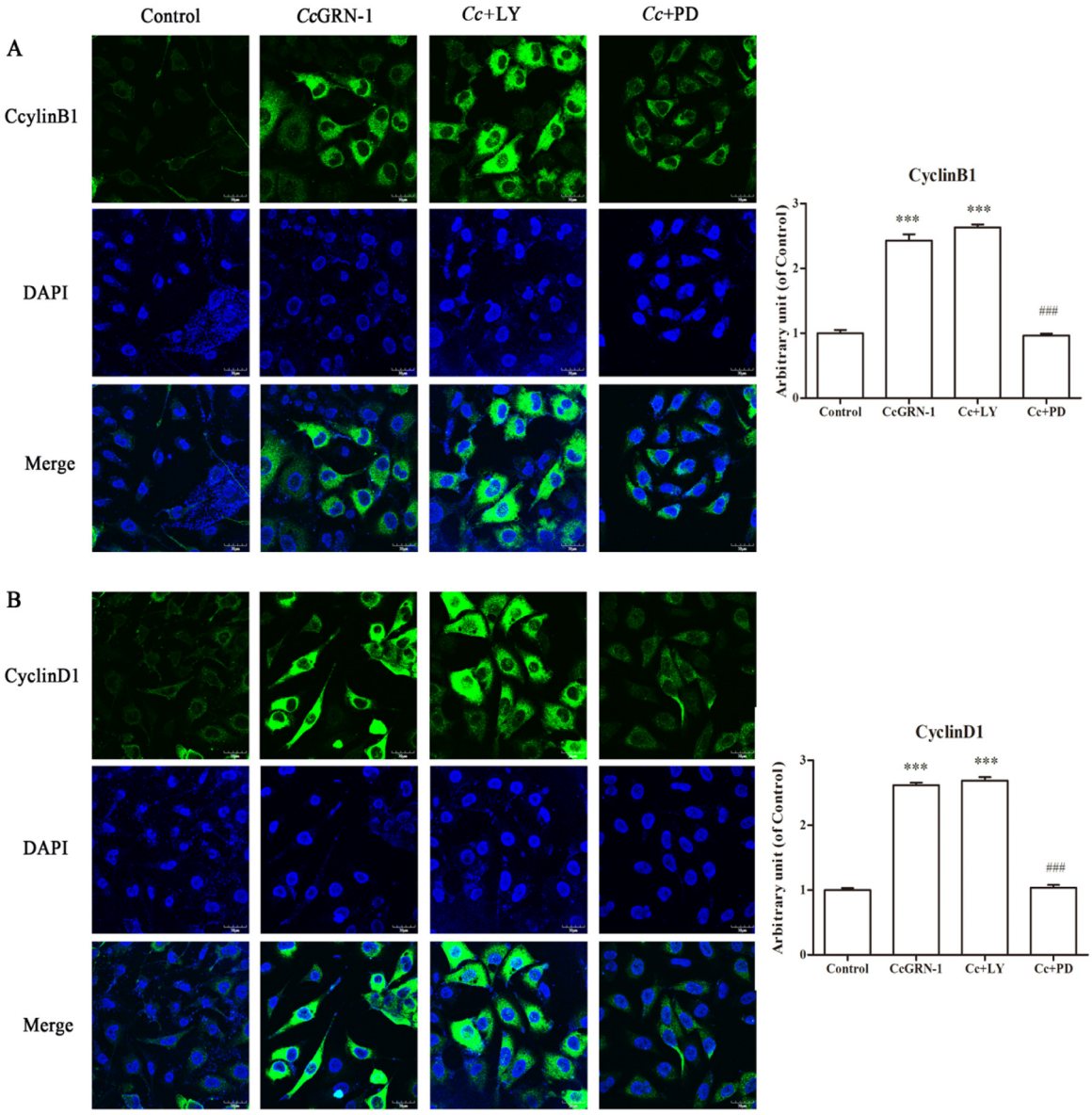

Fig. 9. Effects of signaling-pathway inhibitors on the *Cc*GRN-1-induced expression of CyclinB1 and CyclinD1. A CyclinB1 expression. B CyclinD1 expression. HUVECs were pretreated with *Cc*GRN-1 (0.5 μg/ml) for 30 min in the presence or absence of inhibitors for Akt and ERK1/2 MAPK, respectively. Images were obtained by a fluorescence microscope at 600 × magnification, scale = 30 μm. *Cc: Cc*GRN-1, LY: LY294002, PD: PD98059. $^{***}P < 0.001$ *vs.* Control. $^{\#\#\#}P < 0.001$ *vs. Cc*GRN-1.

short half-life and vulnerability to interference by inflammatory substances. As a marine-derived GRN homologue, *Cc*GRN-1 plays a role in the special environment of seawater which exhibits many undesirable features such as high salt, and osmotic pressure, high quantities of bacteria and low temperature. Thus we expect that *Cc*GRN-1 may have unique advantages over the existing growth factors to overcome their handicap. Further study is needed to assess the half time and other important characters when *Cc*GRN-1 work in unfavorable circumstances. Furthermore, more in-depth experiments, such as animal and clinic trials, also need to be performed to verify the potentials of *Cc*GRN-1 in treating non-healing wounds such as seawater immersion wounds and chronic wounds associated with diabetes, aging and cardiovascular diseases.

5. Conclusion

In this study, we isolated and identified a novel GRN homologue, *Cc*GRN-1, from the jellyfish *C. capillata*. Our results indicated that *Cc*GRN-1 possessed growth-promoting properties, which was associated with the activation of the ERK1/2 signal pathway. To the best of our knowledge, very little is known about the growth factors or their homologues from jellyfish, and *Cc*GRN-1 is the first GRN homologue found in jellyfish, which enriches our understandings of GRNs In general, the results of this study provides a basis for further study of the structure/function relationship and mechanism of action of *Cc*GRN-1. More importantly, as a marine-derived bioactive growth factor, *Cc*GRN-1 may be a good candidate to be developed as a novel wound-healing agent to treat chronic wounds in unfavorable conditions. However, further *in vivo* experiments are needed to verify the potentials of *Cc*GRN-1 in wound treatment in the near future.

Acknowledgements

The authors thank Pro. Huixin Hong from the Fisheries College of Jimei University for his careful identification of the jellyfish species and Mr. Fang Wei from the Foreign Languages' Office of the Second Military Medical University for his careful revision of the manuscript's English language.

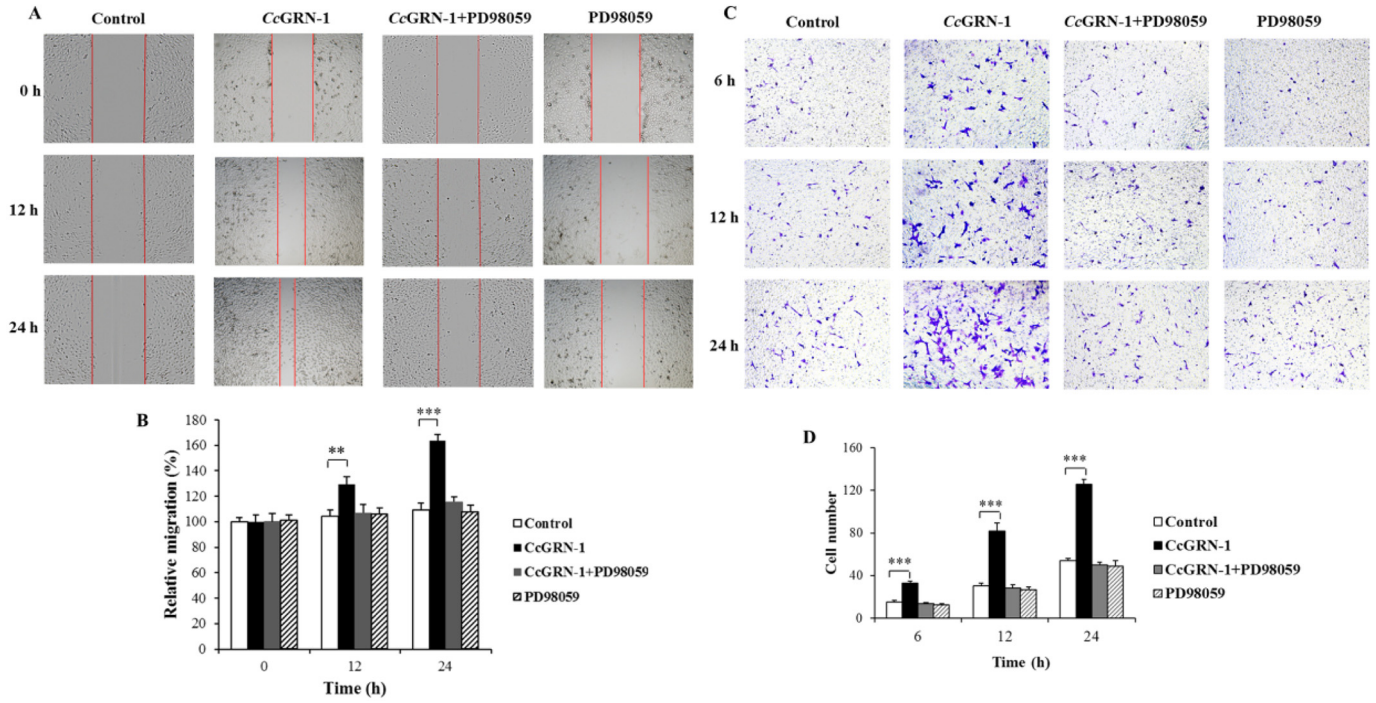

Fig. 10. The ERK1/2 MAPK signaling–pathway was involved in *Cc*GRN-1-induced endothelial cell migration. A HUVECs treated with *Cc*GRN-1 in the presence or absence of the ERK1/2 MAPK inhibitors PD98059, PD98059 directly or PBS as control in a cell-culture wound-healing assay. B Quantitative analysis of the wound-healing assay. Images were obtained by a fluorescence microscope at 100 × magnification. $^{**}P < 0.01$, $^{***}P < 0.001$ *vs.* Control. C Representative images (magnification, ×400) of migratory HUVECs treated as in A. D Migratory cell numbers in five independent fields. $^{***}P < 0.001$ *vs.* Control.

Funding

This work was supported by the National Natural Science Foundation of China (grant number: 81673348).

Ethics approval and consent to participate

Jellyfish outbreaks are increasing in many sea areas in China and have damaged the normal composition and function of marine ecosystems and ecological environments. Thus, catching jellyfish is permitted by the Chinese government.

Declaration of competing interest

The authors declare that they have no conflicts of interest.

Appendix A. Supplementary data

Supplementary data to this article can be found online at https://doi.org/10.1016/j.ijbiomac.2019.05.101.

References

[1] S.A. Eming, P. Martin, M. Tomic-Canic, Wound repair and regeneration: mechanisms, signaling, and translation, Sci. Transl. Med. 6 (2014) 265sr6.
[2] S. Barrientos, O. Stojadinovic, M.S. Golinko, H. Brem, M. Tomic-Canic, Growth factors and cytokines in wound healing, Wound Repair Regen. 16 (2008) 585–601.
[3] S. Barrientos, H. Brem, O. Stojadinovic, M. Tomic-Canic, Clinical application of growth factors and cytokines in wound healing, Wound Repair Regen. 22 (2014) 569–578.
[4] G.C. Gurtner, M.A. Chapman, Regenerative medicine: charting a new course in wound healing, Adv Wound Care (New Rochelle) 5 (2016) 314–328.
[5] S. Werner, R. Grose, Regulation of wound healing by growth factors and cytokines, Physiol. Rev. 83 (2003) 835–870.
[6] S. Malhotra, M.S. Hu, C.D. Marshall, T. Leavitt, A.T. Cheung, J.G. Gonzalez, H. Kaur, H.P. Lorenz, M.T. Longaker, Mesenchymal stromal cells as cell-based therapeutics for wound healing, Stem Cells Int. 2016 (2016) 4157934.
[7] A.J. Whittam, Z.N. Maan, D. Duscher, V.W. Wong, J.A. Barrera, M. Januszyk, G.C. Gurtner, Challenges and opportunities in drug delivery for wound healing, Adv Wound Care (New Rochelle) 5 (2016) 79–88.
[8] E.M. George, H. Liu, G.G. Robinson, F. Mahdi, E. Perkins, G.L. Bidwell, 3rd, Growth factor purification and delivery systems (PADS) for therapeutic angiogenesis, Vasc Cell. 7 (2015) 1.
[9] R. Sable, P. Parajuli, S. Jois, Peptides, Peptidomimetics, and polypeptides from marine sources: a wealth of natural sources for pharmaceutical applications, Mar Drugs 15 (2017) 124.
[10] H.A. Suleria, S. Osborne, P. Masci, G. Gobe, Marine-based nutraceuticals: an innovative trend in the food and supplement industries, Mar Drugs 13 (2015) 6336–6351.
[11] V. Brekhman, A. Malik, B. Haas, N. Sher, T. Lotan, Transcriptome profiling of the dynamic life cycle of the scypohozoan jellyfish Aurelia aurita, BMC Genomics 16 (2015) 74.
[12] J. Schmich, Y. Kraus, D. De Vito, D. Graziussi, F. Boero, S. Piraino, Induction of reverse development in two marine hydrozoans, Int J Dev Biol 51 (2007) 45–56.
[13] D. Gurska, A. Garm, Cell proliferation in cubozoan jellyfish Tripedalia cystophora and Alatina moseri, PLoS One 9 (2014), e102628.
[14] A.L. Primo, S.C. Marques, J. Falcão, D. Crespo, M.A. Pardal, U.M. Azeiteiro, Environmental forcing on jellyfish communities in a small temperate estuary, Mar. Environ. Res. 79 (2012) 152–159.
[15] M. Gordon, J. Seymour, Growth, development and temporal variation in the onset of six Chironex fleckeri medusae seasons: a contribution to understanding jellyfish ecology, PLoS One 7 (2012), e31277.
[16] K.A. Pitt, C.M. Duarte, C.H. Lucas, K.R. Sutherland, R.H. Condon, H. Mianzan, J.E. Purcell, K.L. Robinson, S. Uye, Jellyfish body plans provide allometric advantages beyond low carbon content, PLoS One 8 (2013), e72683.
[17] K. Seipel, M. Eberhardt, P. Muller, E. Pescia, N. Yanze, V. Schmid, Homologs of vascular endothelial growth factor and receptor, VEGF and VEGFR, in the jellyfish Podocoryne carnea, Dev. Dyn. 231 (2004) 303–312.
[18] L. Xiao, J. Zhang, Q.Q. Wang, Q. He, S.H. Liu, Y. Li, L.M. Zhang, In vitro and in vivo haemolytic studies of tentacle-only extract from jellyfish Cyanea capillata, Toxicol. in Vitro 24 (2010) 1203–1207.
[19] G. Liu, Y. Zhou, D. Liu, Q. Wang, Z. Ruan, Q. He, L. Zhang, Global transcriptome analysis of the tentacle of the jellyfish Cyanea capillata using deep sequencing and expressed sequence tags: insight into the toxin- and degenerative disease-related transcripts, PLoS One 10 (2015), e0142680.
[20] R. Yang, G.R. Thomas, S. Bunting, A. Ko, N. Ferrara, B. Keyt, J. Ross, H. Jin, Effects of vascular endothelial growth factor on hemodynamics and cardiac performance, J. Cardiovasc. Pharmacol. 27 (1996) 838–844.
[21] K.E. Johnson, T.A. Wilgus, Vascular endothelial growth factor and angiogenesis in the regulation of cutaneous wound repair, Adv Wound Care (New Rochelle) 3 (2014) 647–661.
[22] B. Wang, D. Liu, C. Wang, Q. Wang, H. Zhang, G. Liu, Q. He, L. Zhang, Tentacle extract from the jellyfish Cyanea capillata increases proliferation and migration of human

umbilical vein endothelial cells through the ERK1/2 signaling pathway, PLoS One 12 (2017), e0189920.
[23] Z. Ruan, G. Liu, B. Wang, Y. Zhou, J. Lu, Q. Wang, J. Zhao, L. Zhang, First report of a peroxiredoxin homologue in jellyfish: molecular cloning, expression and functional characterization of CcPrx4 from Cyanea capillata, Mar Drugs 12 (2014) 214–231.
[24] Z. He, A. Bateman, Progranulin (granulin-epithelin precursor, PC-cell-derived growth factor, acrogranin) mediates tissue repair and tumorigenesis, J Mol Med (Berl) 81 (2003) 600–612.
[25] P. Martin, Wound healing–aiming for perfect skin regeneration, Science 276 (1997) 75–81.
[26] A.J. Singer, R.A. Clark, Cutaneous wound healing, N. Engl. J. Med. 341 (1999) 738–746.
[27] L.F. Brown, K.T. Yeo, B. Berse, T.K. Yeo, D.R. Senger, H.F. Dvorak, L. van de Water, Expression of vascular permeability factor (vascular endothelial growth factor) by epidermal keratinocytes during wound healing, J. Exp. Med. 176 (1992) 1375–1379.
[28] C.J. Powers, S.W. McLeskey, A. Wellstein, Fibroblast growth factors, their receptors and signaling, Endocr. Relat. Cancer 7 (2000) 165–197.
[29] J.L. Richard, C. Parer-Richard, J.P. Daures, S. Clouet, D. Vannereau, J. Bringer, M. Rodier, C. Jacob, M. Comte-Bardonnet, Effect of topical basic fibroblast growth factor on the healing of chronic diabetic neuropathic ulcer of the foot. A pilot, randomized, double-blind, placebo-controlled study, Diabetes Care 18 (1995) 64–69.
[30] P. Shiva Krishna, S. Sudha, K.A. Reddy, F.A. Al-Dhabaan, R.S. Meher, M.A. Prakasham, Singara Charya, Studies on wound healing potential of red pigment isolated from marine Bacterium Vibrio sp, Saudi J Biol Sci 26 (2019) 723–729.
[31] T.G. Sahana, P.D. Rekha, A bioactive exopolysaccharide from marine bacteria Alteromonas sp. PRIM-28 and its role in cell proliferation and wound healing in vitro, Int. J. Biol. Macromol. 131 (2019) 10–18.
[32] S. Sellimi, H. Maalej, D.M. Rekik, A. Benslima, G. Ksouda, M. Hamdi, Z. Sahnoun, S. Li, M. Nasri, M. Hajji, Antioxidant, antibacterial and in vivo wound healing properties of laminaran purified from Cystoseira barbata seaweed, Int. J. Biol. Macromol. 119 (2018) 633–644.
[33] C.-C. Tseng, Y.-C. Lai, T.-J. Kuo, J.-H. Su, P.-J. Sung, C.-W. Feng, Y.-Y. Lin, P.-C. Chen, M.-H. Tai, S.-Y. Cheng, H.-M. Kuo, Z.-H. Wen, Rhodoptilometrin, a crinoid-derived anthraquinone, induces cell regeneration by promoting wound healing and oxidative phosphorylation in human gingival fibroblast cells, Mar Drugs 17 (2019) 138.
[34] M. Pozzolini, E. Millo, C. Oliveri, S. Mirata, A. Salis, G. Damonte, M. Arkel, S. Scarfì, Elicited ROS scavenging activity, photoprotective, and wound-healing properties of collagen-derived peptides from the marine sponge Chondrosia reniformis, Mar Drugs 16 (2018) 465.
[35] A. Veeruraj, L. Liu, J. Zheng, J. Wu, M. Arumugam, Evaluation of astaxanthin incorporated collagen film developed from the outer skin waste of squid Doryteuthis singhalensis for wound healing and tissue regenerative applications, Mat Sci Eng C-MATER 95 (2019) 29–42.
[36] Q.-Q. Ouyang, Z. Hu, Z.-P. Lin, W.-Y. Quan, Y.-F. Deng, S.-D. Li, P.-W. Li, Y. Chen, Chitosan hydrogel in combination with marine peptides from tilapia for burns healing, Int. J. Biol. Macromol. 112 (2018) 1191–1198.
[37] A. Bateman, H. Bennett, Granulins: the structure and function of an emerging family of growth factors, J. Endocrinol. 158 (1998) 145–151.
[38] H. Wang, Y. Sun, S. Liu, H. Yu, W. Li, J. Zeng, C. Chen, J. Jia, Upregulation of progranulin by helicobacter pylori in human gastric epithelial cells via p38MAPK and MEK1/2 signaling pathway: role in epithelial cell proliferation and migration, FEMS Immunol. Med. Microbiol. 63 (2011) 82–92.
[39] G. Sparro, G. Galdenzi, A.M. Eleuteri, M. Angeletti, W. Schroeder, E. Fioretti, Isolation and N-terminal sequence of multiple forms of granulins in human urine, Protein Expr. Purif. 10 (1997) 169–174.
[40] G.D. Plowman, J.M. Green, M.G. Neubauer, S.D. Buckley, V.L. McDonald, G.J. Todaro, M. Shoyab, The epithelin precursor encodes two proteins with opposing activities on epithelial cell growth, J. Biol. Chem. 267 (1992) 13073–13078.
[41] Z. He, C.H.P. Ong, J. Halper, A. Bateman, Progranulin is a mediator of the wound response, Nat. Med. 9 (2003) 225–229.
[42] J. Zhu, C. Nathan, W. Jin, D. Sim, G.S. Ashcroft, S.M. Wahl, L. Lacomis, H. Erdjument-Bromage, P. Tempst, C.D. Wright, A. Ding, Conversion of proepithelin to epithelins: roles of SLPI and elastase in host defense and wound repair, Cell 111 (2002) 867–878.
[43] M. Shoyab, V.L. McDonald, C. Byles, G.J. Todaro, G.D. Plowman, Epithelins 1 and 2: isolation and characterization of two cysteine-rich growth-modulating proteins, Proc. Natl. Acad. Sci. U. S. A. 87 (1990) 7912–7916.
[44] D. Tolkatchev, S. Malik, A. Vinogradova, P. Wang, Z. Chen, P. Xu, H.P. Bennett, A. Bateman, F. Ni, Structure dissection of human progranulin identifies well-folded granulin/epithelin modules with unique functional activities, Protein Sci. 17 (2008) 711–724.
[45] M.J. Smout, J. Sotillo, T. Laha, A. Papatpremsiri, G. Rinaldi, R.N. Pimenta, L.Y. Chan, M.S. Johnson, L. Turnbull, C.B. Whitchurch, P.R. Giacomin, C.S. Moran, J. Golledge, N. Daly, B. Sripa, J.P. Mulvenna, P.J. Brindley, A. Loukas, Carcinogenic parasite secretes growth factor that accelerates wound healing and potentially promotes neoplasia, PLoS Pathog. 11 (2015), e1005209.
[46] R. Daniel, E. Daniels, Z. He, A. Bateman, Progranulin (acrogranin/PC cell-derived growth factor/granulin-epithelin precursor) is expressed in the placenta, epidermis, microvasculature, and brain during murine development, Dev. Dyn. 227 (2003) 593–599.
[47] J.C. Chen, B.B. Lin, H.W. Hu, C. Lin, W.Y. Jin, F.B. Zhang, Y.A. Zhu, C.J. Lu, X.J. Wei, R.J. Chen, NGF accelerates cutaneous wound healing by promoting the migration of dermal fibroblasts via the PI3K/Akt-Rac1-JNK and ERK pathways, Biomed. Res. Int. (2014) (2014), 547187.
[48] R. Hrabal, Z. Chen, S. James, H.P. Bennett, F. Ni, The hairpin stack fold, a novel protein architecture for a new family of protein growth factors, Nat. Struct. Biol. 3 (1996) 747–752.
[49] J. Scott, M. Urdea, M. Quiroga, R. Sanchez-Pescador, N. Fong, M. Selby, W.J. Rutter, G.I. Bell, Structure of a mouse submaxillary messenger RNA encoding epidermal growth factor and seven related proteins, Science 221 (1983) 236–240.
[50] A. Gray, T.J. Dull, A. Ullrich, Nucleotide sequence of epidermal growth factor cDNA predicts a 128,000-molecular weight protein precursor, Nature 303 (1983) 722–725.